SLAC–PUB–95–6738

GLAST*

Elliott D. Bloom

Representing the GLAST Team†

Stanford Linear Accelerator Center

Stanford University, Stanford, CA 94309

Invited talk presented at the International Heidelberg Workshop on TeV Gamma Ray Astrophysics, Heidelberg, Germany, October 3-7, 1994

*Work supported by Department of Energy contract DE–AC03–76SF00515.

†GLAST Team members and their institutions are listed in the references.

1 Introduction

Recent results from the Energetic Gamma-Ray Experiment Telescope (EGRET) aboard the Compton Observatory have generated strong interest in space based high-energy ($E_\gamma > 10$ MeV) gamma ray astronomy. This science has wetted our curiosity of what might be observed with an instrument having considerably more capability than EGRET, if such a device were practical in our fiscally difficult times. Advances in silicon technology over the past decade, and the resulting rapid drop in costs, encourage the development of a dramatically new type of high-energy gamma ray space telescope based on silicon strip technology. The GLAST team [1] (GLAST stands for Gamma-ray Large Area Space Telescope) has been working for the past two years on the design of such an instrument, and the development of the silicon strip hardware and readout electronics needed to realize our design. Figure 1 shows an artist's concept of our current instrument design, including the spacecraft. As in previous high-energy instruments, GLAST is a pair spectrometer backed by a total absorption electro-magnetic shower counter. Measurement of the energy and direction of the induced electro-magnetic shower provides information about the energy and direction of the incident gamma-ray. However, due to the flexibility and relatively low cost of the silicon strip technology, the telescope has about a factor of 10 increase in effective area over EGRET, and about a factor of 5 increase in field of view. At the same time, the GLAST design is calculated to have much better point source sensitivity, and to have an energy range of

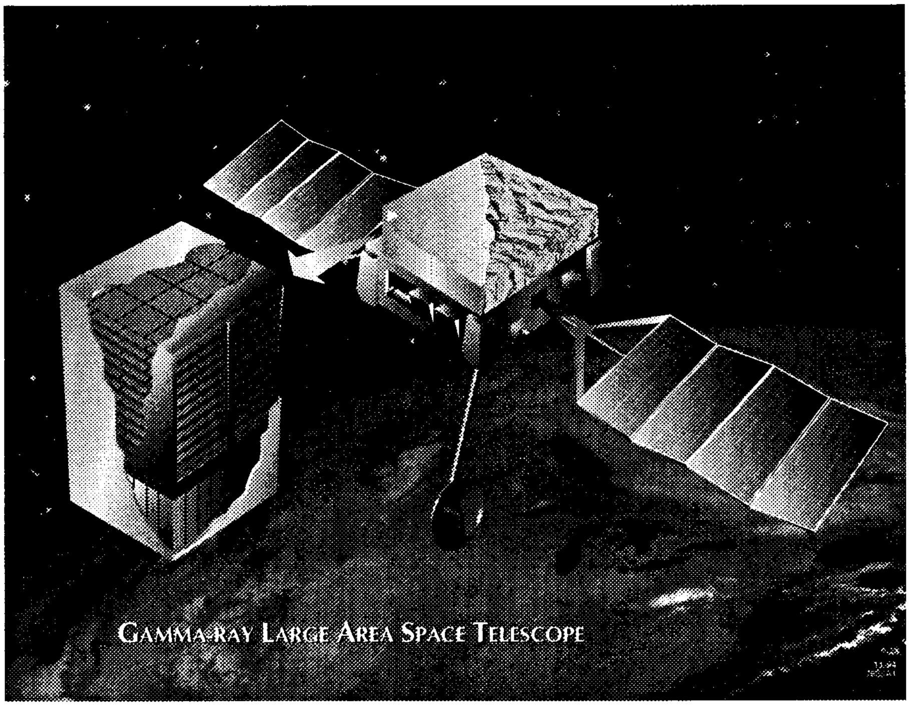

Figure 1: An artist's conception of the GLAST detector and spacecraft in orbit. The picture also shows an exploded view of one tower of the 49 in the current design.

10 MeV $< E_\gamma <$ 300 GeV. Due to the economies of silicon technology, along with weight, and size savings compared to gas based detector technology, we estimate that this instrument can be built and flown as a Delta II mission. Thus, GLAST would easily fit into the NASA intermediate mission category with an estimated total cost of about \$200 million.

2 The GLAST Design

Figure 2 shows some details of the current GLAST design. The telescope consists of three elements: a segmented charged particle anticoincidence shield; a gamma-ray tracker/converter, consisting of thin sheets of high-Z converter material interspersed with silicon strip detectors for particle tracking; and a segmented 10 r.l. CsI calorimeter to provide good energy resolution at high energies. As the top part of Figure 2 shows, and by the arrow in Figure 1, the GLAST detector is modular, consisting of a 7×7 array of towers, with each tower containing elements of the anticoincidence shield, the tracker/converter stack, and the calorimeter. The bottom part of Figure 2 shows, along with the tracker/converter, a longitudinally segmented calorimeter design that can dramatically increase the effective area of the detector at high energy by using the photon angle measurement from the calorimeter alone. Such design details of the calorimeter, as well as other aspects of the detector, are still in development.

Note that the detector technology we are using naturally allows GLAST to be wide (W) compared to its depth (D). This results from having no separate time of flight system in the GLAST design. The powerful self-triggering and tracking capabilities of the silicon strip technology obviate the need for TOF. Figure 3(a) shows the instrument acceptance versus aspect ratio (W/D), where W and D are defined in part (b) of the figure. The large aspect ratio of GLAST greatly increases its angular acceptance, i.e., fraction of the sky seen at one time, compared to previous instruments (EGRET is shown for example in the figure).

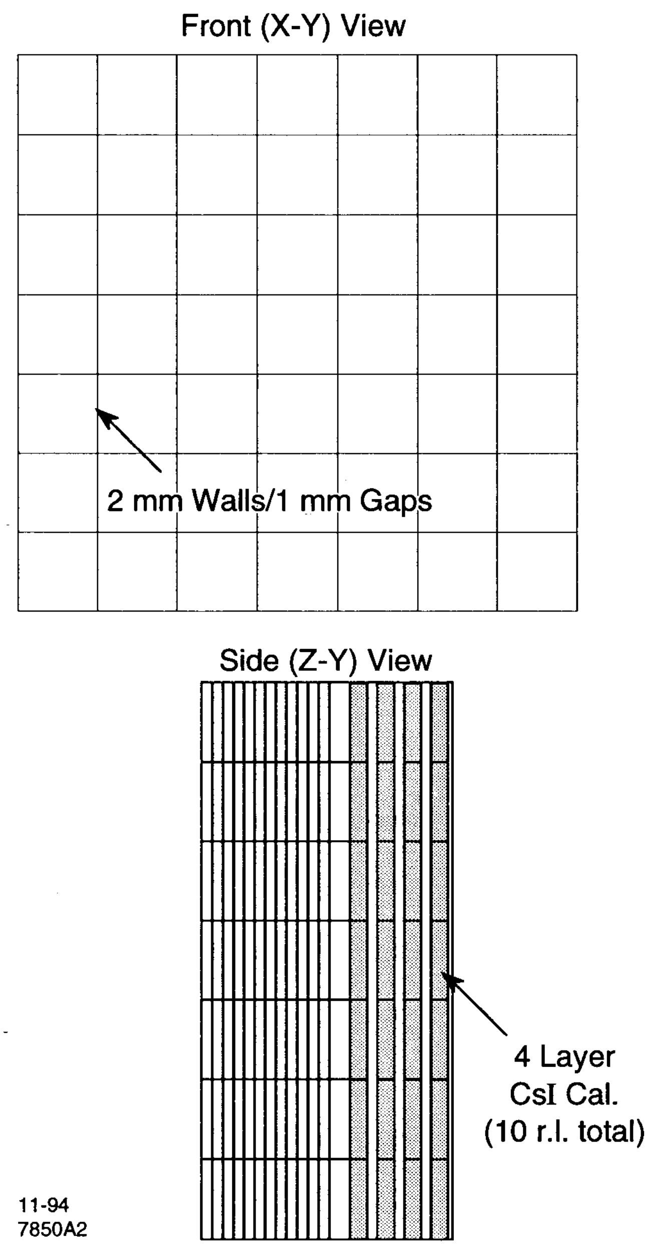

Figure 2: A detailed view of the GLAST detector geometry in plan or front (top part of figure) and side (bottom part of figure) views.

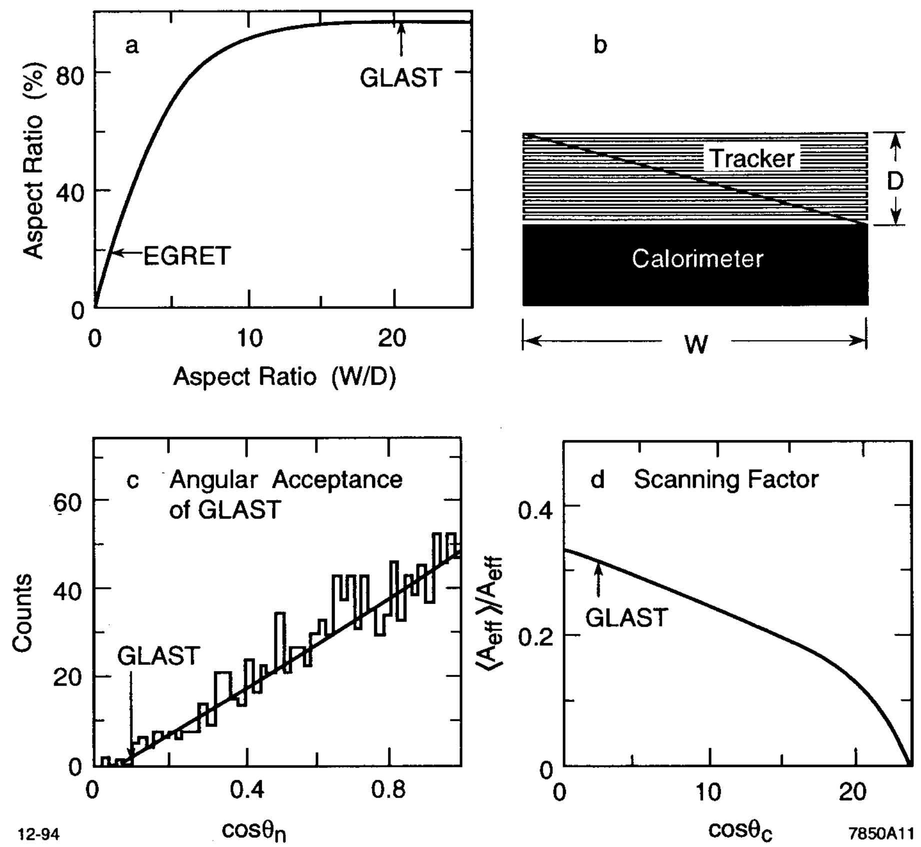

Figure 3: Part (a) shows the instrument acceptance versus aspect ratio (W/D), where W and D are defined in part (b) of the figure. Part (c) shows the relative angular acceptance of GLAST versus the cosine of the angle to normal incidence to the detector, $\cos\Theta_n$. The GLAST cutoff angle, $\cos\Theta_c$, is about 0.1. Part (d) shows an effective "scanning factor" vs $\cos\Theta_c$. The scanning factor gives the normalized effective area of the instrument, when the spacecraft is operating in anti-nadir pointing mode, over one full orbit (see text).

Part (c) of the figure shows the relative angular acceptance of GLAST versus the cosine of the angle to normal incidence to the detector. The detector cutoff angle, $\cos\Theta_c$, is about 0.1. The large angular acceptance of GLAST, combined with normal spacecraft operation in orbit that is anti-nadir pointing, allows great sensitivity to transient events. This is quantified in part (d) of Figure 3, which shows an effective "scanning factor" versus $\cos\Theta_c$. The scanning factor gives the normalized effective area of the instrument, when the spacecraft is operating in anti-nadir pointing mode, over one full orbit. Thus, any object in the sky that is seen with A_{eff} when it is at maximum acceptance has a scanning factor of, $< A_{eff} > / A_{eff}$, where

$$\frac{\langle A_{eff}\rangle}{A_{eff}} = \frac{1}{2\pi}\int_{-\Theta_c}^{\Theta_c} \frac{\cos\Theta_{orb} - \cos\Theta_c}{1-\cos\Theta_c} d\Theta_{orb}. \tag{1}$$

GLAST views any object in the sky, within its acceptance, with about 1/3 of the object's maximum acceptance in GLAST averaged over one orbit ($\sim$ 90 minutes). Of course, depending on the orbit, some parts of the sky may never be seen in this mode.

2.1 The Tracker

The gamma-ray tracker/converter, in the current GLAST design, consists of a tracking layer of silicon strips that provides a charged particle anticoincidence veto, followed by 10 radiator/tracking layers of 0.05 radiation lengths each, spaced 3 cm apart, and finally an additional 2 tracking layers, also spaced 3 cm apart. Behind each radiator is a tracking layer consisting of a pair of single-sided silicon strip detectors that provide (x, y) position determination. Downstream of these 10 layers are two planes of (x, y) single-sided silicon strip detectors. These last two layers without radiator are used to track the previously converted photons. As three points are a minimum needed to establish a track, radiator in these layers will just degrade tracking performance, with no gain in acceptance.

The 240 μm strip pitch will result in a rms position resolution of about 70 μm in x and y. The e^- and e^+ from a just converted photon will make one hit in the silicon immediately following the radiator, thus precisely locating the conversion point. The multiple scattering occurring in the radiator and the intrinsic opening angle of the pair will typically cause two hits in the next layer of silicon (which is after the next radiator). Multiple scattering in the second radiator has a minor effect on the determination of the direction of the tracks since it is located directly on top of the second layer of silicon. The intrinsic two-hit resolution of 480 μm allows for more accurate tracking of the initial pair than in gaseous tracking devices in which the two-hit resolution is typically 2–3 mm.

For very high energy photons, the rms projected angular resolution of this configuration is limited to about 0.03° by the strip pitch and spacing between planes. For the total of 0.56-radiation-length thickness of the tracker/converter, the probability of a photon converting is 0.35 (above 1 GeV).

Large arrays (smaller than GLAST) of silicon strip detectors have been built and successfully operated as elements of particle physics detectors.

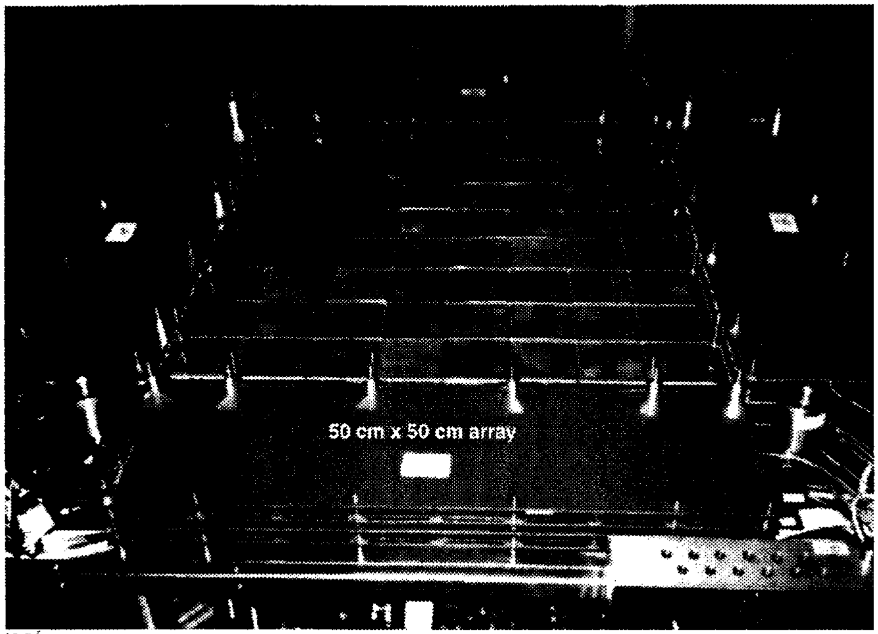

Figure 4: A picture of the Wizard Collaboration[3] silicon strip multilayer detector flown on a balloon. Each layer is a 50 cm by 50 cm array.

These devices typically operate in radiation fields that are larger than those expected to be seen by the GLAST instrument. Figure 4 shows a multilayer silicon strip detector array built and flown in a balloon by the Wizard collaboration [2]. This device operated successfully.

2.2 The Calorimeter

The photon energy is estimated by measuring the $e^{\pm}$ shower energy deposited in the calorimeter and correcting for energy losses in the tracker/converter (currently estimated by hit counting). The calorimeter must provide good energy resolution in the energy range from 10 MeV to about 100 GeV, and reasonable energy resolution to about 300 GeV. It must be coarsely pixelated in order to aid in the rejection of backgrounds. Readout is via photodiodes. Current design calls for a 10-radiation-length calorimeter, with a longitudinal segmentation by 4 and a transverse size of 3×3 cm. This results in an array of 64×4 crystals for each GLAST tower, or 12,544 for the entire detector. Thallium-doped cesium iodide is the material of choice in the current design. CsI(Tl) provides excellent energy resolution at modest cost, has a short radiation length (1.86 cm), and Moliere radius (3.8 cm), and provides a signal that is fast for our purposes. This material is also reasonably radiation hard. In addition, larger (compared to GLAST) CsI detectors have been built and operated as elements of particle physics detectors. The practicality of longitudinal segmentation is currently under review.

In summary, the GLAST design has many technical benefits including:

- no consumables
- all relatively low voltages
- modularity
- modern, low cost, robust, and long-lived technology

It also has its design challenges including a large channel count of about 10^6 channels and on-board computing requirements. We believe that we currently have viable designs that meet these challenges.

3 Estimated GLAST Performance

High-energy gamma rays from space are excellent probes of the most energetic phenomena that occur in nature. They are emitted over a wide range of angular scales from a diverse population of astrophysical sources: stellar mass objects, in particular neutron stars and black hole candidates; the nuclei of active galaxies (AGN) which are likely to contain massive black holes; interstellar gas in the galaxy that interacts with high energy cosmic rays; the diffuse extragalactic background; supernovae that may be sites of cosmic ray acceleration; and gamma-ray bursts. Many of these sources exhibit transient phenomena.

3.1 Comparison of EGRET to GLAST

Interest in these areas has received a large boost from the EGRET instrument over the past 2 years, with more yet to come. A sample of EGRET results includes [5]:

- Pulsed gamma-ray emission above 100 MeV detected from 5 pulsars.
- More than 30 sources detected in the galactic plane, including high energy gamma emission from the galactic center region.
- Diffuse emission detected from the Large Magellanic Cloud. This observation along with nondetection of the Small Magellanic Cloud, directly shows that cosmic rays are not universal but are galactic in origin.

- Gamma-ray emission from more than 40 AGN. These have variability observed on time scales of days to months. Ground based observations from 0.5 TeV on up of Mkn 421 by the Whipple observatory have been coordinated with observation by EGRET. Recently a flare of Mkn 421 was simultaneously observed by ASCA, CGRO and Whipple.

- More than 25 high-latitude unidentified sources.

- Several high-energy gamma-ray bursts detected. One burst lasted more than 90 minutes with emission to at least 18 GeV.

- Detection of a solar flare of several hours duration and emission to at least 2 GeV.

GLAST can make a dramatic improvement on EGRET observations. Due to its larger effective area and field of view, lower energy threshold, and deadtimeless operation, GLAST will be much more sensitive to transient events. (The use of spark chambers in EGRET introduces a 0.1 second deadtime per event.) Figure 5 and Table 1 compare EGRET to our current GLAST design. The figure shows the relative sizes of the two instruments. The weight of GLAST allows the instrument to be launched on a Delta II class rocket. The table details a comparison of a number of important observational and other parameters for the two instruments.

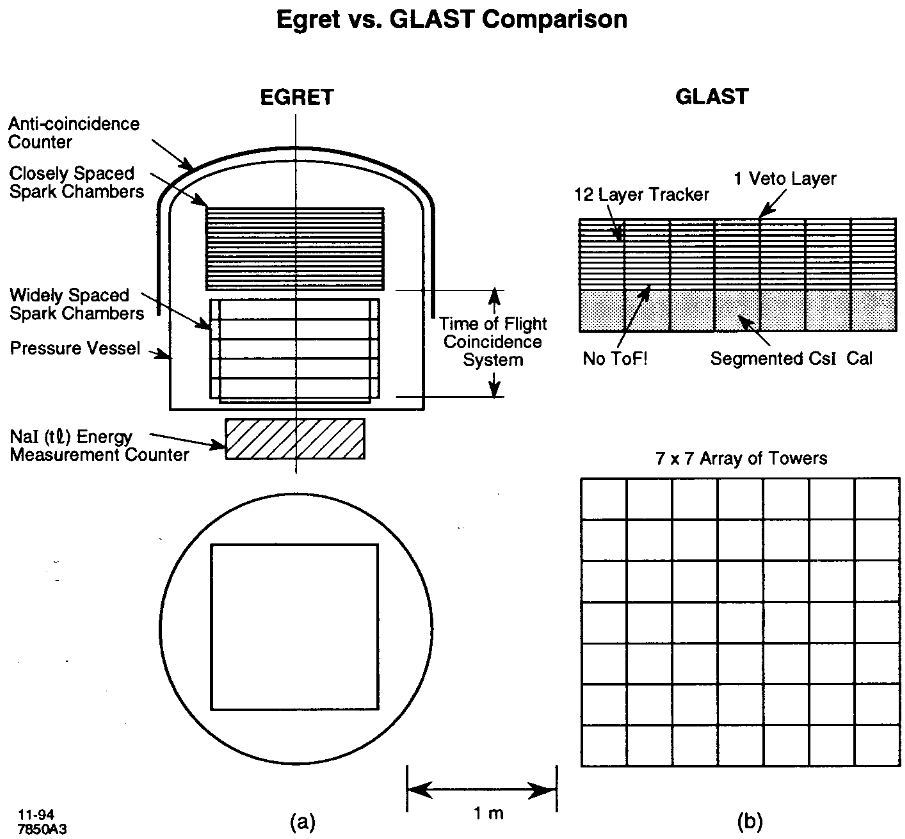

Figure 5: A comparison of the physical sizes of EGRET and GLAST to the same scale. A meter is shown in the figure for comparison. The major subsystems of each detector are also enumerated in the figure. Given its small size and relatively light weight, GLAST can be launched on a Delta II rocket.

3.2 GLAST Performance

One of the main challenges in operating a gamma-ray detector in space is control of the backgrounds in the detector. One expects that many charged and neutral particles (cosmic-ray protons, ions, electrons, Earth albedo gamma-rays,

Table I. Comparison of GLAST and EGRET γ-ray Telescope Parameters.

	EGRET$^{(1)}$	GLAST Conceptual Design
Energy range	35 MeV–30 GeV$^{(2)}$	$\sim$ 10 MeV–300 GeV
Energy resolution$^{(3)}$		
10 MeV	...	24%
50 MeV	14%	12%
100 MeV	12%	8%
1 GeV	9%	4.4%
10 GeV	12%	6%
100 GeV	...	18%
Effective Area$^{(4)}$		
10 MeV	...	300 cm^2
50 MeV	250 cm^2	4000 cm^2
1 GeV	1200 cm^2	8000 cm^2
10 GeV	700 cm^2	8000 cm^2
100 GeV	...	8000 cm^2
Solid Angle Acceptance$^{(5)}$	$0.15 \times \pi$ sr	$0.82 \times \pi$ sr
Full Field of View	$0.2 \times \pi$ sr	$1.8 \times \pi$ sr
Point Source Sensitivity$^{(6)}$		
E > 100 MeV	5.4×10^{-8} ph cm^{-2} s^{-1}	1.5×10^{-9} ph cm^{-2} s^{-1}
E > 1 GeV	1.2×10^{-8} ph cm^{-2} s^{-1}	1.5×10^{-10} ph cm^{-2} s^{-1}
E > 10 GeV	2.1×10^{-8} ph cm^{-2} s^{-1}	9.5×10^{-10} ph cm^{-2} s^{-1}
Single photon position$^{(7)}$		
50 MeV	8.4 deg	5.2 deg
100 MeV	5.6 deg	2.5deg
1 GeV	1.5 deg	0.42 deg
10 GeV	0.5 deg	0.1 deg
Point Source Location	5–10 arcmin	0.1–1 arcmin
Volume$^{(8)}$	4.8 m^3	$\sim$ 2 m^3
Mass	1830 kg	$\sim$ 2700 kg
Power	190 W	$\sim$ 1 kW
Lifetime	$\sim$ 4 yr	> 4 yr

(1) Parameters for the EGRET instrument are from Refs. [4,5].

(2) This is the energy range when the EGRET trigger system is operated with the NaI calorimeter (TASC) in coincidence. This is the normal operating mode. With TASC not in coincidence, the energy range is 20 MeV to about 30 GeV. This latter mode is not normally used because of the higher rate of spark chamber gas consumption.

(3) Equivalent Gaussian σ. For EGRET, both the e^- and e^+ enter the calorimeter for the resolutions shown.

(4) Area $\times$ γ-ray detection efficiency. The effective areas given for GLAST include γ-ray detection inefficiencies due to background rejection analysis cuts. The geometric area of GLAST is 28,200 cm^2. For comparison, the geometric area of the EGRET spark chamber is 6,400 cm^2.

(5) FWHM. The effective area at the edge of the field is 50% of its on-axis value.

(6) T his is the flux sensitivity at a 5σ detection threshold. The background assumed is 2×10^{-5} photons cm^{-2} s^{-1} sr^{-1} (100 MeV/E)$^{1.1}$, typical of the background seen by EGRET at high galactic latitudes. In each case, the exposure assumed is that obtained from a 1 year all-sky survey.

(7) Angle for 68% containment from a point source. The high energy angular resolution of GLAST is determined by the spacing between converter planes, the radiation lengths per converter, and the pitch of the Si strips. For the numbers shown here, the spacing between planes is 3.0 cm, the converters are each 0.05 radiation lengths thick, and the readout pitch is 240 μm ($\sigma = 69\mu$m).

(8) The volume and mass estimates do not include the spacecraft.

neutrons, trapped radiation, etc.) will interact with GLAST and its spacecraft. The flux of cosmic gamma-rays is very small in comparison. One of the most difficult problems is the observation of the diffuse extragalactic gamma-ray flux, which is approximately 10^4 smaller in rate than cosmic rays at the same energy. The GLAST trigger system initially provides information for all of these events, which can be used to reject a large fraction of the background events.

While the overall initial data rate could be accepted by modern accelerator based particle physics detectors, this data volume would be prohibitive to downlink to the ground from GLAST. In order to minimize the onboard computing requirements, while limiting sufficiently the data downlink rate, the event processing for GLAST is done in several steps:

- Hardware coincidences between adjacent layers of silicon, using programmable gate arrays. This level 1 trigger is expected to run at about 5 kHz.

- Basic pattern recognition (track finding) using the on board computers. This level 2 trigger includes fast analysis of the veto layers, and is calculated to run at 30 Hz or lower. Simulations show that level 2 reduces the cosmic ray rate by a factor of better than 200. This level of onboard computing is modest and can be accomplished with about 15 MIPS of computing. At this level about 100 Kbits/sec would have to be downlinked to the ground.

- The use of additional event information, including the pattern of energy deposition in the calorimeter. This level 3 trigger requires more on-board computing power. Simulations indicate that event filtering at this level reduces the downlink rate to 25 Kbits/sec, a very comfortable rate.

- The rest of the background events to be excluded on the ground to a level of at least one part in 10^5. The events downlinked will undergo extensive computer analysis to further reduce the background. For the diffuse isotropic extragalactic gamma-rays, with $E_\gamma > 100$ MeV, we have calculated a signal to noise of about 20 to 1.

The initial cosmic ray spectrum is generated using the NRL code called CREME [6]. For the analysis presented here, we generated 200 K cosmic ray events. Figure 6(a) shows the generated cosmic ray proton spectrum after veto cuts. After our additional standard set of simulation cuts, Figure 6(b) results. There is one event with a "measured" $E_\gamma > 100$ MeV left in the spectrum. Using a cosmic ray rate of 0.17 cm^2/sec, integrated over the GLAST acceptance, and an extragalactic diffuse isotropic γ rate of 2×10^{-5} cm^2/sec/sr for $E_\gamma > 100$ MeV, we find a signal to noise of 19.6 to 1. Additional rejection techniques, currently under development, may improve this by about a factor of 10.

Figure 7(a) shows an EGRET all sky map on which is superimposed the GLAST field of view and the EGRET field of view. A dramatic improvement is evident from EGRET to GLAST. Part (b) of the figure shows the single

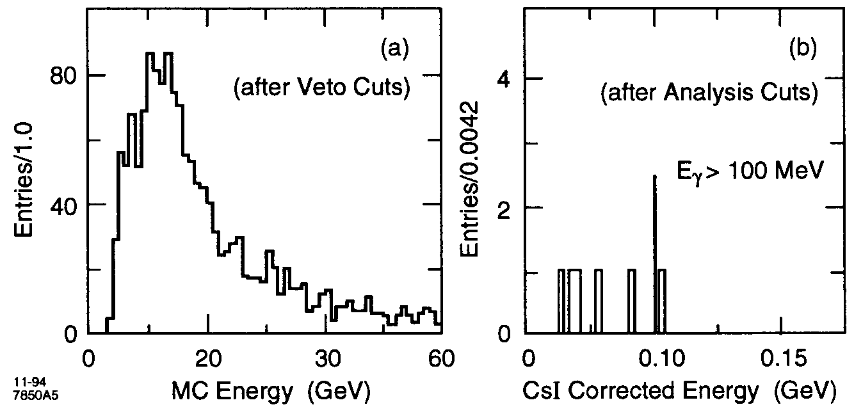

Figure 6: 200 K cosmic ray events are generated using the CREME [6] code. Part (a) shows the generated cosmic ray proton spectrum after veto cuts. After our additional standard set of simulation cuts, part (b) results. There is one event with a "measured" $E_\gamma > 100$ MeV left in the spectrum.

photon projected angle versus energy for GLAST and EGRET. Part (c) of the figure shows the effective area of GLAST, EGRET, and GLAST when using the γ angle measurement from the segmented calorimeter. The flat high energy acceptance of GLAST is achieved by eliminating the veto of good γ events from their charged particle "backsplash". This effect is what limits the high energy acceptance of EGRET due to its monolithic veto "dome". One sees an increase of an additional factor of about 3 in the GLAST effective area by using the segmented calorimeter photon angle measurements. This improvement is important at high γ energy where the rate is low.

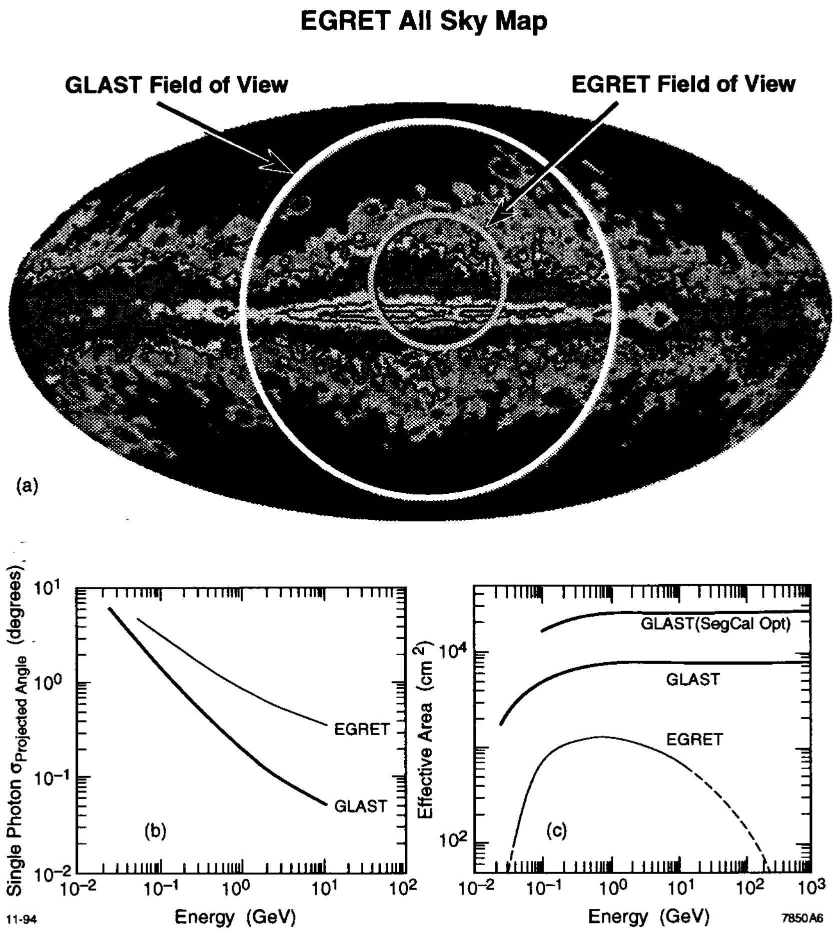

Figure 7: Part (a) shows an EGRET all sky map on which is superimposed the GLAST field of view and the EGRET field of view. A dramatic improvement is evident from EGRET to GLAST. Part (b) shows the single photon projected angle vs energy for GLAST and EGRET. Part (c) shows the effective areas of GLAST, EGRET, and GLAST when using the γs that interact in the tracker or just in the calorimeter.

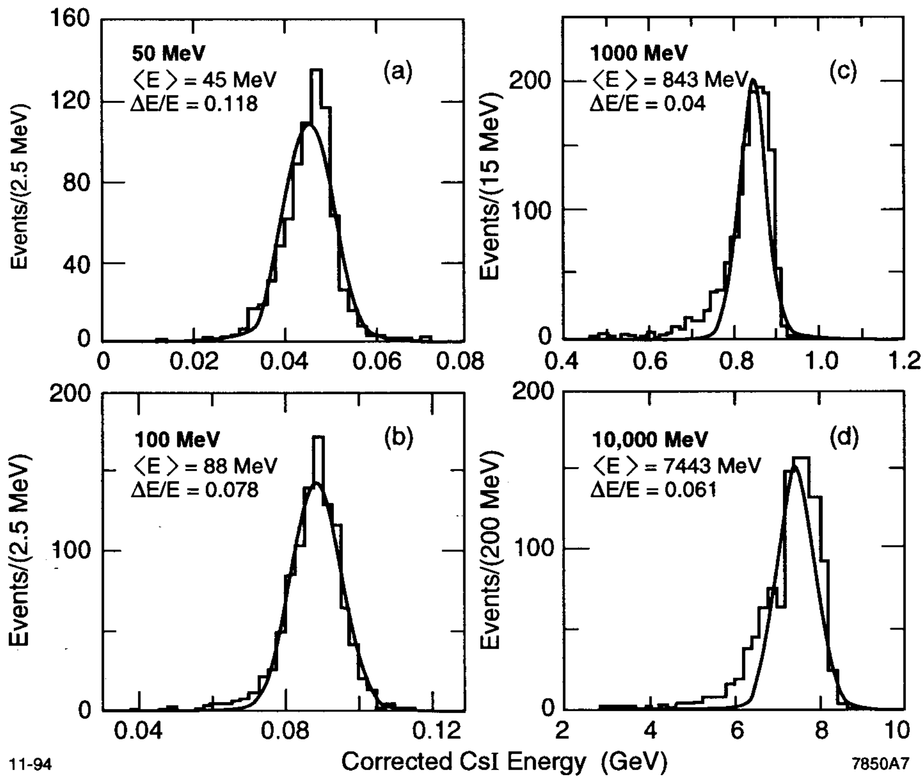

Figure 8: The MC distributions for photons in the GLAST calorimeter; parts (a) through (d) show 50 to 10,000 MeV.

Figure 8 shows the MC distributions for photons in the GLAST calorimeter; parts (a) through (d) show 50 to 10,000 MeV. At 300 GeV, the energy resolution is about 25%, which is adequate for these highest energies.

Figure 9 even more dramatically shows the power of the GLAST detector. The top part of the figure repeats the EGRET all sky map, with the GLAST (and EGRET) field of view centered on the molecular cloud Rho Ophiuchas. The bottom part of the figure explodes the view of this source using the full detail

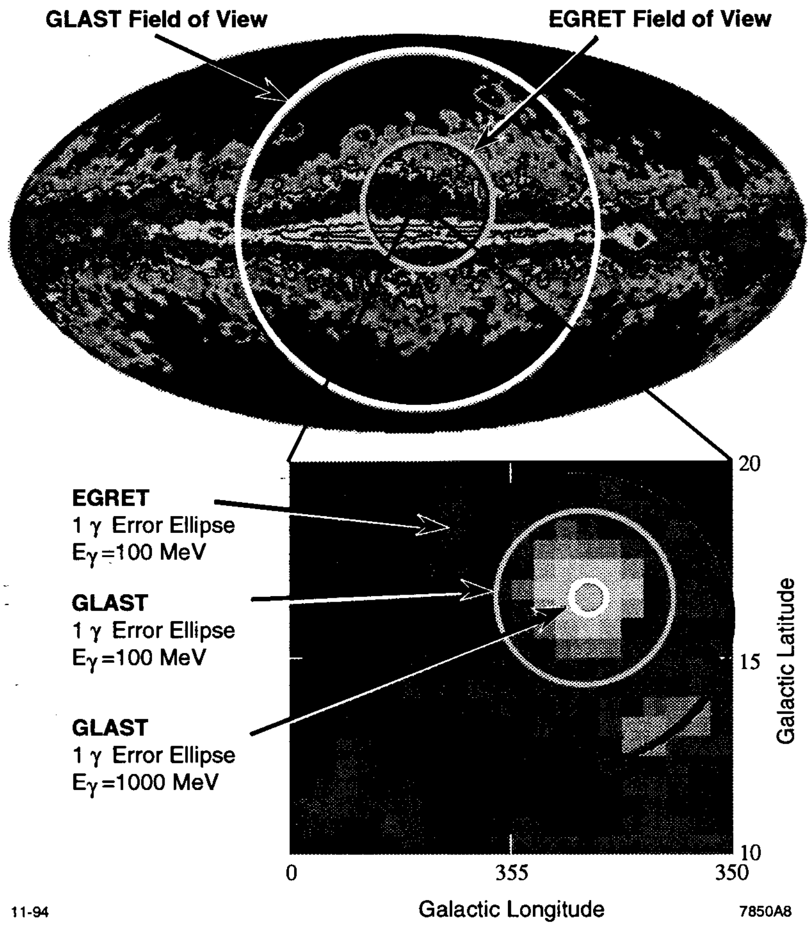

Figure 9: The top part of the figure shows the EGRET all sky map, with the GLAST and EGRET fields of view centered on the molecular cloud Rho Ophiuchas. The bottom part of the figure explodes the view. The outer circle shows the achieved EGRET single photon 1 σ position error ellipse at 100 MeV. The next (grey) ellipse in shows the GLAST single photon resolution at the same energy. However, the (white) innermost ellipse gives the GLAST single photon resolution at 1 GeV. At 1 GeV GLAST contains as many photons in this ellipse as does EGRET in its 100 MeV ellipse.

of the EGRET map. The outer circle shows the achieved EGRET single photon $1\ \sigma$ position error ellipse at 100 MeV. This ellipse quantifies the relative two source resolution of the detector. The next (grey) ellipse in shows the GLAST single photon resolution at the same energy. However, the (white) inner most ellipse gives the GLAST single photon resolution at 1 GeV. At 1 GeV GLAST contains as many photons in this ellipse as does EGRET in its 100 MeV ellipse.

Figure 10 demonstrates this spectacular GLAST resolution (combined with area) in the simulation of results for an all-sky (anti-nadir pointing mode) 1 year GLAST survey ($E_\gamma > 100$ MeV). In the top half of the map, the simulation

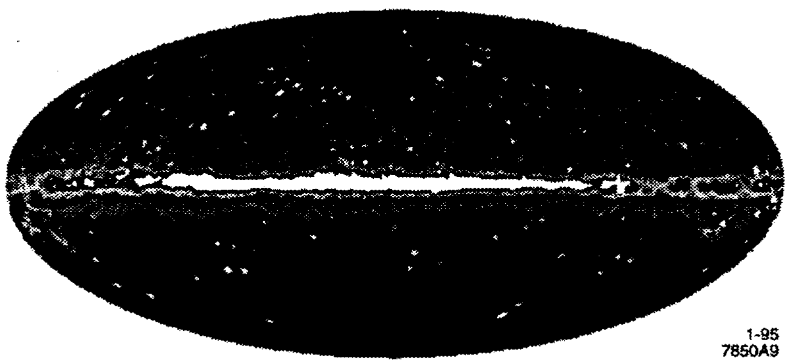

Figure 10: A galactic coordinate projection of the sky from a GLAST detector simulation. Included in the top half is the galactic diffuse background, plus extragalactic (the known EGRET sources, plus extrapolated sources as discussed in the text). The bottom half of the map has the galactic diffuse background, plus extragalactic (the known EGRET sources, plus diffuse background). The Galactic plane is overexposed in this false "grayscale" image.

extrapolates the ln(N) versus ln(S) plot for AGN to lower S as $N(S > S_0) \sim S^{-3/2}$. Included is the galactic diffuse background, plus extragalactic (the known EGRET sources, plus AGN using the above extrapolation for N). The bottom half of the map has the galactic diffuse background, plus extragalactic (the known EGRET sources, plus 100% diffuse background). The Galactic plane is overexposed in the false "grayscale" image. With no special processing, the raw image is shown, the difference between top and bottom half is clear (even though the black and white reproduction of the image is poor).

3.3 Connections to the ground based observation program

As mentioned previously, the Whipple observatory has cooperated with the CGRO team and others in coordinating space based and ground based observations of high energy gamma-rays [7]. The GLAST team hopes this activity will expand to a worldwide scale when GLAST is in orbit. The major mode of GLAST observations will be in the anti-nadir scanning mode (some pointed observations may also be made). In this mode GLAST will scan most of the sky once per orbit. If a transient of interest should be observed, Earth based observation stations could be contacted very quickly. Figure 11 demonstrates how this might work. Figure 11(a) shows the GLAST uncorrected point spread function obtained with a $1/E^2$ input photon spectrum. We assume such an energy dependence for Mkn 421 within the GLAST energy range. As part (a) of the figure shows, 68% of the photons are contained within about 2.5°

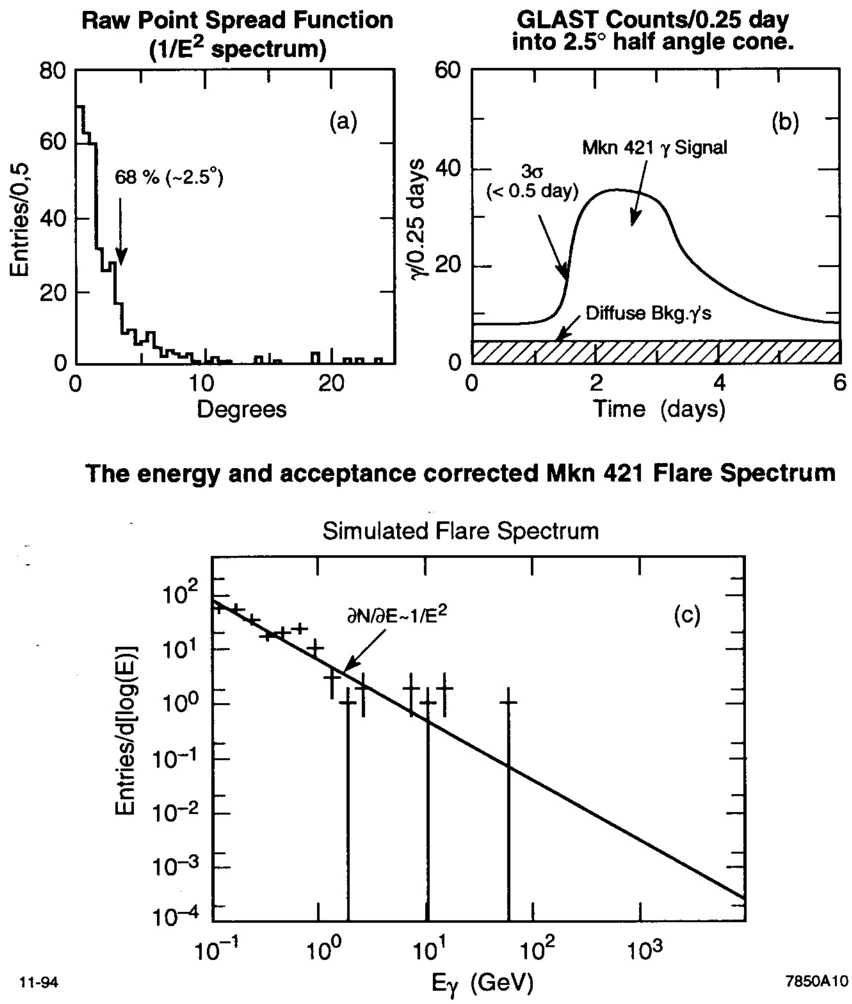

Figure 11: Part (a) plots the raw point spread function of GLAST for a $1/E^2$ incident photon spectrum. 68% of the photons are contained within about 2.5° (half-angle). Part (b) of the figure shows a simulated flare of Mkn 421 consistent with past flares. The ordinate plots GLAST counts/0.25 day into a 2.5° half-angle cone. Part (c) shows the simulated flare spectrum as observed in GLAST. This spectrum includes events during the flare, from about day 1.5 to day 5.

(half-angle). Part (b) of the figure shows a simulated flare of Mkn 421, beginning at the start of day 1.5, consistent with past flares. As the figure shows, a 3σ effect for the source flare is seen in less than 0.5 day by GLAST. Part (c) shows the simulated flare spectrum as observed in GLAST. This spectrum includes events from about day 1.5 to day 5. There is useful information in this spectrum to about 10 GeV. If quickly brought on line, the ground based instruments should be able to obtain useful information from about 100 GeV upwards to a few TeV. Note that an extended observation, e.g., 1 year in anti-nadir pointing mode, by GLAST of this source, assuming the source is not flaring during this time, should yield only ~ 6 events > 100 GeV, assuming the same $1/E^2$ spectrum as in part (c) of the figure.

4 Summary and Conclusions

High-energy astronomy in orbit has generated great interest due to recent results from EGRET. The GLAST team is developing the next generation γ-ray telescope, GLAST, that would extend the EGRET discovery reach by about 2 orders of magnitude. This impressive improvement is due to a number of factors:

- much larger effective area
- "full" sky view
- factor of 30 in energy reach (10 MeV $< E_\gamma <$ 300 GeV)
- rapid transient response in anti-nadir scanning mode
- much better source resolution
- much longer lifetime in space due to no consumables

GLAST can be built quickly and relatively inexpensively due to its use of modern silicon technology. This technology is in hand as evidenced by its extensive use in large particle physics experiments, the balloon flight of the Wizard collaboration prototype, and the space flight of small detectors by a number of missions.

In addition to its direct contribution to space based γ-ray astronomy, GLAST would significantly contribute to ground based γ-ray astronomy, which works at significantly higher energy, by enabling a fast response to transient phenomenon by the ground based telescopes.

Given all of these factors, we believe that GLAST represents an unusually urgent scientific opportunity that should be realized within this decade.

Acknowledgments

I would like to thank Bill Atwood for extensive discussions and comments.

References

[1] The GLAST Team currently consists of the following institutions and individuals, in alphabetical order by institution: University of Chicago—Corbin Couvault, Rene Ong, Mark Oreglia; Kanagawa University—Katsuaki Kasahara; Lockheed Research Laboratory, Palo Alto, CA—David Chenette; Los Alamos National Laboratory—Geoffrey Mills; University of Maryland—John Mattox; Max Planck Institut für Extraterrestriche Physik—Hans Mayer-Hasselwander; NASA Ames Reasearch Center—Jeffrey Scargle; Naval Research Laboratory—Eric Grove, Paul Hertz, W. Neil Johnson, Michael Lovellette, Gerald Share, Kent Wood; University of California at Santa Cruz—Robert Johnson; Sonoma State University—Lynn Cominsky; Stanford University—(Physics Department and HEPL) Yin-Chi Lin, Peter Michelson, Patrick Nolan, Arthur Walker, Jr., (Stanford Linear Accelerator Center) William Atwood, Elliott Bloom, Michael Chen, Gary Godfrey, Alex Luebke, (Aero-Astro Department) Robert Twiggs; University of Tokyo—Tuneyoshi Kamae; Instituto Nazionale di Fisica Nucleare, Trieste—Guido Barbiellini, Alberto Colavita; University of Washington—Thompson Burnett.

[2] Picture and information provided courtesy of G.Barbiellini, A. Colavita, INFN, Trieste, members of the Wizard Collaboration.

[3] Peter Michelson, Private Communication.

[4] D. J. Thompson et al., Ap. J. Suppl. **86**, 629 (1993).

[5] A. H. Walker, Ph.D. thesis, Stanford University, Stanford, California (1990).

[6] CREME code, James A. Adams, Naval Research Laboratory, Washington, DC. To be found on EnviroNET, Mail Code 410.1, NASA Goddard Space Flight Center, Greenbelt, MD 20771.

[7] Trevor Weeks, Private Communication.